CHEMISTRY OF MATERIALS
Article

Chem. Mater. **2010,** *22,* 5271–5278 5271
DOI:10.1021/cm101408n

In Situ Crystallization of Macroporous Monoliths with Hollow NaP Zeolite Structure

Yi Huang,[†] Dehua Dong,[†] Jianfeng Yao,[†] Li He,[†] Jenny Ho,[†] Chunhua (Charlie) Kong,[‡] Anita J. Hill,[§] and Huanting Wang*[,†]

[†]*Department of Chemical Engineering, Monash University, Clayton, VIC 3800, Australia,* [‡]*Electron Microscope Unit, University of New South Wales, Sydney, NSW 2052, Australia, and* [§]*Commonwealth Scientific and Industrial Research Organization (CSIRO), Materials Science and Engineering, Private Bag 33, Clayton South, VIC 3169, Australia*

Received May 19, 2010. Revised Manuscript Received July 14, 2010

Macroporous NaP zeolite monoliths (M-ZPMs) with designed shapes such as cylinder, rectangular-prism, and donut shapes were synthesized via gelcasting of the aged zeolite gel with colloidal silica as a binder and subsequent vapor-phase-transport (VPT) synthesis. X-ray diffraction (XRD), scanning electron microscopy (SEM), mercury porosimetry, and nitrogen gas adsorption were used to characterize the samples at different synthesis stages. SEM images revealed that the resulting macroporous NaP zeolite monoliths were composed of interconnected hollow particles. Mercury porosimetry showed that the macroporous NaP zeolite monoliths possessed bimodal macropore size distributions involving the textural macropores (ca. 100 μm) and skeletal macropores (ca. 3.5 μm). Furthermore, colloidal silica played a crucial role in the formation of robust macroporous NaP zeolite monoliths. Specifically, as the mass loading of colloidal silica in the zeolite-gel monoliths increases, the mechanical strength and Si/Al ratio of the resulting zeolitic monoliths increased; dispersible and individual hollow NaP zeolite particles with lower Si/Al ratios were produced in the absence of colloidal silica. The formation mechanisms of the hollow NaP zeolites in the VPT synthesis process were discussed. The incorporation of functional magnetic Fe_3O_4 in M-ZPMs was finally presented.

Introduction

Zeolites with hierarchical porous structures have been widely studied, because of their selectivity and improved kinetics in catalysis, adsorption, and separation processes.[1−11] Zeolites containing mesopores,[1−3,12] macropores,[4,5,7−15] or both mesopores and macropores[7,12] have shown significant improvement in the diffusion of guest molecules, thus substantially reducing the transport resistance. To date, several synthesis strategies have been developed to prepare hierarchical porous zeolite structures, including artificial/biological hard-/soft-/dual-templating synthesis,[1,4,9−13,16−18] self-assembly of preformed zeolite nanocrystals,[8,14] post-synthesis creation of an extra pore system,[2] and direct zeolitization of hierarchical porous silica materials.[15,19] A variety of hierarchical porous zeolites such as silicalite,[7,9,10,13,14,16] ZSM-5,[1,2,4] FAU,[3,8] and BEA[8,20−22] have been reported so far. For instance, silicalite zeolite monoliths with ordered macroporous structures were fabricated by

*Author to whom correspondence should be addressed. Tel.: +61-3-9905-3449. Fax: +61-3-9905-5686. E-mail: huanting.wang@eng.monash.edu.au.

(1) Choi, M.; Cho, H. S.; Srivastava, R.; Venkatesan, C.; Choi, D. H.; Ryoo, R. *Nat. Mater.* **2006**, *5*, 718–723.
(2) Groen, J. C.; Zhu, W. D.; Brouwer, S.; Huynink, S. J.; Kapteijn, F.; Moulijn, J. A.; Perez-Ramirez, J. *J. Am. Chem. Soc.* **2007**, *129*, 355–360.
(3) Huang, Y.; Wang, K.; Dong, D. H.; Li, D.; Hill, M. R.; Hill, A. J.; Wang, H. T. *Microporous Mesoporous Mater.* **2010**, *127*, 167–175.
(4) Anderson, M. W.; Holmes, S. M.; Hanif, N.; Cundy, C. S. *Angew. Chem., Int. Ed.* **2000**, *39*, 2707–2710.
(5) Dong, A. G.; Ren, N.; Yang, W. L.; Wang, Y. J.; Zhang, Y. H.; Wang, D. J.; Hu, H. H.; Gao, Z.; Tang, Y. *Adv. Funct. Mater.* **2003**, *13*, 943–948.
(6) El-Nafaty, U. A.; Mann, R. *Chem. Eng. Sci.* **1999**, *54*, 3475–3484.
(7) Wang, H. T.; Huang, L. M.; Wang, Z. B.; Mitra, A.; Yan, Y. S. *Chem. Commun.* **2001**, 1364–1365.
(8) Huang, L. M.; Wang, Z. B.; Sun, J. Y.; Miao, L.; Li, Q. Z.; Yan, Y. S.; Zhao, D. Y. *J. Am. Chem. Soc.* **2000**, *122*, 3530–3531.
(9) Holland, B. T.; Abrams, L.; Stein, A. *J. Am. Chem. Soc.* **1999**, *121*, 4308–4309.
(10) Valtchev, V. *Chem. Mater.* **2002**, *14*, 4371–4377.
(11) Wang, Y. J.; Tang, Y.; Dong, A. G.; Wang, X. D.; Ren, N.; Gao, Z. *J. Mater. Chem.* **2002**, *12*, 1812–1818.
(12) Valtchev, V. P.; Smaihi, M.; Faust, A. C.; Vidal, L. *Chem. Mater.* **2004**, *16*, 1350–1355.
(13) Dong, A. A.; Wang, Y. J.; Tang, Y.; Zhang, Y. H.; Ren, N.; Gao, Z. *Adv. Mater.* **2002**, *14*, 1506.
(14) Rhodes, K. H.; Davis, S. A.; Caruso, F.; Zhang, B. J.; Mann, S. Chem. Mater. **2000**, *12*, 2832-+.
(15) Tong, Y. C.; Zhao, T. B.; Li, F. Y.; Wang, Y. *Chem. Mater.* **2006**, *18*, 4218–4220.
(16) Valtchev, V.; Smaihi, M.; Faust, A. C.; Vidal, L. *Angew. Chem., Int. Ed.* **2003**, *42*, 2782–2785.
(17) Zhang, B. J.; Davis, S. A.; Mendelson, N. H.; Mann, S. *Chem. Commun.* **2000**, 781–782.
(18) Han, L.; Yao, J. F.; Li, D.; Ho, J.; Zhang, X. Y.; Kong, C. H.; Zong, Z. M.; Wei, X. Y.; Wang, H. T. *J. Mater. Chem.* **2008**, *18*, 3337–3341.
(19) Mintova, S.; Holzl, M.; Valtchev, V.; Mihailova, B.; Bouizi, Y.; Bein, T. *Chem. Mater.* **2004**, *16*, 5452–5459.
(20) Naydenov, V.; Tosheva, L.; Sterte, J. *Chem. Mater.* **2002**, *14*, 4881–4885.
(21) Song, J. W.; Ren, L. M.; Yin, C. Y.; Ji, Y. Y.; Wu, Z. F.; Li, J. X.; Xiao, F. S. *J. Phys. Chem. C* **2008**, *112*, 8609–8613.
(22) Valtchev, V.; Mintova, S. *Microporous Mesoporous Mater.* **2001**, *43*, 41–49.

Published on Web 09/01/2010

simple sedimentation of seeded mesoporous silica spheres in a mold, followed by hydrothermal transformation.[13] Wang and co-workers reported that hierarchical porous silicalite tubes with well-controlled microstructures and designed shapes were prepared by applying the ceramic gelcasting technique, followed by high-temperature treatment to remove the polymer binder and sinter zeolite nanocrystals together.[7] Note that the high-temperature calcination commonly used for removal of organic templates/binders and sintering often leads to decreased crystallinity of zeolites. Until now, there have been few studies on controlling the shapes of these zeolitic monoliths with good mechanical stability.[9,13,14,21] Therefore, it would be of great interest to pursue an effective fabrication method, which is capable of controlling the porosity, mechanical strength, and shape of hierarchically porous zeolite monoliths.

In this paper, we report our work on the synthesis of mechanically stable, macroporous NaP zeolite monoliths with hollow particle structures. To the best of our knowledge, there has been no report on the synthesis of NaP zeolitic monoliths with macroporous and hollow structures without using any "sacrificial templates". P-type zeolite has a gismondine (GIS) framework topology with intersecting channels of 0.31 nm × 0.44 nm in [100] and 0.26 nm × 0.49 nm in [010].[23−25] The micropore size of P-type zeolite is smaller than that of FAU, LTA, MFI, and BEA zeolites, which makes P-type zeolite useful for the separation of very small gas or liquid molecules.[24,25] Furthermore, P-type zeolite is also useful for the removal/immobilization of toxic and radioactive waste species (Cs, Sr, Ba, Pb, and U),[23,26] heavy metals/ammonium removal from wastewaters,[27,28] seawater potassium extraction,[29] and the formation of environmentally friendly detergent.[30] In the present work, the synthesis method for forming macroporous NaP zeolite monoliths involves gelcasting of the sufficiently aged zeolite gel with colloidal silica as "nutrient binder" and in situ crystallization of the shaped zeolite-gel monolith by VPT synthesis. The monolith with a desirable shape can be readily achieved by constructing a suitable casting mold. The in situ crystallization, without using a secondary template via VPT synthesis, ensured successful retaining of the shape of the monolith; after the crystallization process, and consumption of the silica binder, macroporous NaP zeolite monoliths composed of interconnected hollow NaP zeolites were produced. By contrast, without the addition of colloidal silica, dispersible hollow NaP zeolite particles were prepared. In addition, magnetic Fe_3O_4 nanoparticles were successfully encapsulated in hollow NaP zeolite structures of the monolith.

Experimental Section

Materials. The chemicals used in our study are as follows: sodium hydroxide pellets (99%, Sigma−Aldrich), aqueous colloidal silica (Ludox HS-30, 30%, Sigma−Aldrich), aluminum isopropoxide (98%, Sigma−Aldrich), acrylamide (AM, 99%, Sigma−Aldrich), *N*,*N*′-methylenebisacrylamide (MBAM, 98%, Sigma−Aldrich), ammonium persulfate ($(NH_4)_2S_2O_8$, 98%, Sigma−Aldrich)), iron(II, III) oxide (< 50 nm, Sigma−Aldrich) and doubly deionized (DDI) water. All chemicals were directly used without further purification.

Preparation of Aged Zeolite Gel. The aged zeolite gel was prepared with a molar composition of $9.6Na_2O$:$1.0Al_2O_3$:$14.4SiO_2$:$288.8H_2O$, under the slightly modified synthetic conditions described in our previous paper.[3] Typically, a sodium hydroxide solution was prepared by mixing 9.49 g of sodium hydroxide with 37.50 g of DDI water in a clean polypropylene bottle. After the complete dissolution of sodium hydroxide, 5.00 g of aluminum isopropoxide was added under vigorous agitation for 2 h. The resulting sodium aluminate solution was mixed thoroughly with 35.25 g of colloidal SiO_2 solution (Ludox HS-30) to yield a sodium aluminosilicate gel. The bottle with the sodium aluminosilicate gel was then tightly sealed and stirred at a constant rate of 650 rpm for 24 h at room temperature, followed by a secondary aging process, i.e., at 58 ± 1 °C for 40−45 h. After the secondary aging, the zeolite gel was collected by centrifugation and repeatedly washing with DDI water until the pH value of the decanted solution was ∼13.0−13.5. The resulting aged zeolite gel was then dried at room temperature for 24 h and further at 60 °C for 36 h. The dried zeolite gel was ground to a powder before use.

Gelcasting of the Aged Zeolite Gel. A suspension with a solids loading of 30−35 wt % was prepared for gelcasting, and its composition (by weight) was 28.302−33.019 ($x$$SiO_2$:1(zeolite gel)), 1.698−1.981 (8AM:2MBAM:1$(NH_4)_2S_2O_4$), and 65−70H_2O, where x is 0, 0.1, 0.2, and 0.3. Typically, when x is 0.2, 10 g of aged zeolite gel powder were dispersed in 18.956 g of DDI water, followed by mixing with 6.667 g of Ludox HS-30 (2 g of SiO_2), 0.131 g of MBAM, and 0.524 g of AM. The mixture was thoroughly mixed via ball milling for 36 h, to get a stable homogeneous zeolite silica-gel suspension. Then, 1.091 g of a $(NH_4)_2S_2O_8$ aqueous solution (6 wt %) was added under stirring for 5 min to complete the total solids loading of 34 wt %. The suspension was degassed in an ultrasonic bath for 5−10 min, to release the trapped air bubbles, and then carefully transferred to a homemade multihole Teflon mold; polymerization of the monomers (AM and MBAM) was carried out at 60 °C for 12 h under N_2. The solidified zeolite-gel monoliths were quickly unmolded and further dried in a tube furnace at 50 °C for 24 h and 60 °C for 48 h. The dried zeolite-gel monoliths were finally sintered in air at 500 °C for 8 h with a heating rate of 1 °C/min to remove the organic polymers. The dried zeolite-gel monoliths and sintered zeolite-gel monoliths with different silica loadings were designated as ZGM-x and S-ZGM-x (x = 0, 0.1, 0.2, and 0.3), respectively. In our study, ZGMs and S-ZGMs with cylinder (1 cm in diameter × 1.5−2 cm in length), rectangular-prism (1 cm × 1 cm × 2 cm) and donut (1 cm inner diameter (ID) × 2 cm outer diameter (OD)) shapes were fabricated.

(23) Atkins, M.; Glasser, F. P.; Jack, J. J. *Waste Manage.* **1995**, *15*, 127–135.
(24) Dong, J. H.; Lin, Y. S. *Ind. Eng. Chem. Res.* **1998**, *37*, 2404–2409.
(25) Yin, X. J.; Zhu, G. S.; Wang, Z. Y.; Yue, N. L.; Qiu, S. L. *Microporous Mesoporous Mater.* **2007**, *105*, 156–162.
(26) Nery, J. G.; Mascarenhas, Y. P.; Cheetham, A. K. *Microporous Mesoporous Mater.* **2003**, *57*, 229–248.
(27) Haron, M. J.; Ab Rahim, F.; Abdullah, A. H.; Hussein, M. Z.; Kassim, A. *Mater. Sci. Eng. B* **2008**, *149*, 204–208.
(28) Querol, X.; Moreno, N.; Umana, J. C.; Juan, R.; Hernandez, S.; Fernandez-Pereira, C.; Ayora, C.; Janssen, M.; Garcia-Martinez, J.; Linares-Solano, A.; Cazorla-Amoros, D. *J. Chem. Technol. Biotechnol.* **2002**, *77*, 292–298.
(29) Cao, J. L.; Liu, X. W.; Fu, R.; Tan, Z. Y. *Sep. Purif. Technol.* **2008**, *63*, 92–100.
(30) Araya, A.; Adams, C. J.; Graham, P.; Hight, A. T. Use of aluminosilicates of the zeolite p type as low temperature calcium binders, U.S. Patent 5,560,829, October 1, 1996.

In Situ Crystallization of S-ZGMs. A quantity of 0.5−1.5 g of the S-ZGM-x were first immersed in water under vacuum for incipient wetness, and then placed in a raised stainless steel mesh cup in the Teflon-lined autoclave with sufficient water on the bottom. The autoclave was tightly sealed and heated at 150 °C for 2−5 days to crystallize the S-ZGM-x. After VPT synthesis, macroporous zeolite NaP monolith (denoted M-ZPM) was dried under ambient laboratory conditions for 2−3 days before characterization.

Incorporation of Magnetic Particles into M-ZPM. The M-ZPM incorporated with a functional guest species such as Fe_3O_4 was demonstrated in this work. Similar procedures were applied to fabricate the monolith, except that a designed amount of Fe_3O_4 (2−4 wt % of the total weight of zeolite gel and silica) was added during preparation of zeolite gel−silica suspension. The ball-milling time was extended to 2−3 days, ensuring the homogeneous mixing of zeolite gel, silica, and Fe_3O_4 nanoparticles. After the casting process, the color of the monoliths was dark brown, which changed to red brown after sintering. VPT synthesis was also prolonged to 3−4 days to completely crystallize the monoliths.

Characterization. Powder X-ray diffraction (XRD) analysis was performed using a Philips PW1140/90 diffractometer with a Cu Kα target (40 kV, 25 mA), a 2θ range of 5°−60° at a scan rate of 1°/min and a step size of 0.02°. The XRD patterns were indexed according to the standard FAU and NaP diffraction patterns listed on the International Zeolite Association website (http://www.iza-online.org/). Scanning electron microscopy (SEM) micrographs were obtained with a JEOL Model JSM-6300FE scanning electron microscope (15/30 kV). The energy-dispersive X-ray spectrometry (EDXS) device attached to the SEM system was used to conduct elemental analysis of the samples. The distribution of iron(II, III) oxide among the hollow zeolite NaP structures was determined by performing EDXS (line scan) of broken zeolite NaP particles located on the fractured surface of monoliths using a JEOL Model JSM-7001FE scanning electron microscope (15 kV) that was equipped with an EDXS device. Nitrogen sorption experiments were performed at 77 K with a Micromeritics Model ASAP 2020MC analyzer. The samples were degassed at 250 °C for 10 h prior to analysis, and the specific surface areas were calculated according to the Brunauer−Emmett−Teller (BET) method.

The cross-sectional microscopy analyses of zeolite particles were carried out with a FEI Model xT Nanolab 200 Nova Dualbeam FIB focused-ion-beam system. The powder samples were dispersed in ethanol via ultrasonication for 30 s. A drop of the suspension was taken with a pipet, and a single layer of individual particles was evenly deposited onto a conductive carbon tape after drying, followed by coating with an ∼40-nm-thick layer of gold in an Emitech K550x sputter coater. The selected particles, with typical surface morphology, were sectioned with a fine Ga ion beam in the Dualbeam FIB. Prior to ion milling, a 500-nm-thick layer and a 2-μm-wide strap of platinum was deposited in situ on the top surface of the particle to prevent the round edge effects and enhance the conductivity. The rough cross-sectional milling was performed at 30 kV and 1 nA, followed by a cleaning process with a lower beam current. The electron-beam-generated secondary electron images were recorded at 45° with the built-in function of tilt correction.

Results and Discussion

Sample Characterization. The zeolite-gel monoliths (ZGM-x), sintered zeolite-gel monoliths (S-ZGM-x) and macroporous zeolite NaP monoliths (M-ZPM-x, where x = 0.1, 0.2, and 0.3) were characterized by XRD and SEM. The precursor gel for the synthesis of FAU zeolite was chosen to produce the aged zeolite gel, because its metastability promotes a fast phase transformation toward the target NaP zeolite, and it is easily synthesized at low temperatures (e.g., 25−60 °C) without requiring any structure directing agents (SDAs).[3,31] In our study, a two-stage aging was conducted to ensure that the aged gel has a chemical composition (1.67Si/1Al/1.15Na/7.05O, molar ratio) that is similar to that of FAU zeolite.[3] The XRD pattern shown in Figure 1a reveals very weak FAU diffraction peaks at 2θ angles of 6.19° (111), 10.11° (220), 10.86° (311), 15.61° (331), 23.58° (533), and 31.31° (555) (see Figure 1a and the inset).[3,31,32] As an example of sintered aged-zeolite gelcasts, the XRD pattern of S-ZGM-0.2 is shown in Figure 1b. After sintering, the characteristic FAU diffraction peaks of S-ZGM-0.2 disappear, because of the low thermal stability of small crystallites (Figure 1b). XRD patterns of the resulting M-ZPMs indicate that only pure NaP zeolites were produced after VPT synthesis (see Figures 1c−e). In particular, as seen from the intense XRD diffraction peaks, the monoliths with aged zeolite gel and silica were well-crystallized to NaP zeolite.

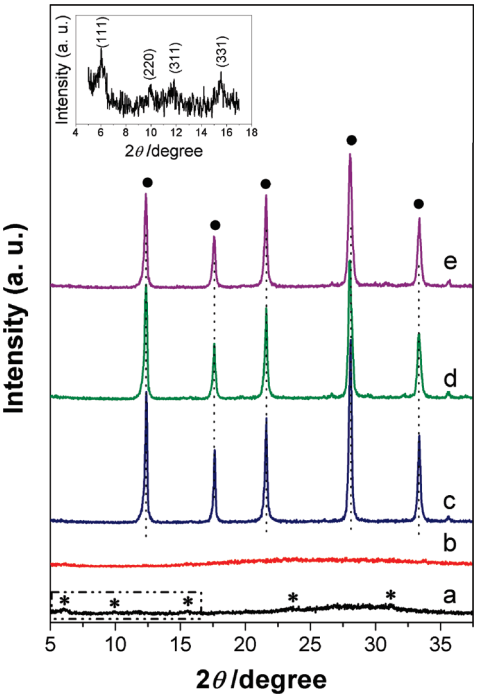

Figure 1. XRD patterns of (a) dried zeolite gel, (b) S-ZGM-0.2, (c) M-ZPM-0.1, (d) M-ZPM-0.2, and (e) M-ZPM-0.3. The inset shows the enlarged XRD pattern of the dried zeolite gel in the 2θ angle range of 5°−17°. (Asterisk (∗) denotes FAU zeolite and solid circle (●) denotes NaP zeolite.)

The photographs of typical examples of ZGM-0.2, S-ZGM-0.2, and M-ZPM-0.2 with a cylinder shape are

(31) Mintova, S.; Olson, N. H.; Bein, T. *Angew. Chem., Int. Ed.* **1999**, *38*, 3201–3204.
(32) Valtchev, V. P.; Bozhilov, K. N. *J. Phys. Chem. B* **2004**, *108*, 15587–15598.

shown in Figures 2a−c. All samples retained the cylinder shape and underwent a total linear shrinkage of 8%−12% in the drying process, and 1%−3% during sintering; M-ZPM-0.2 experienced a small linear expansion (< 1%) during crystallization. The dimension and shape of the M-ZPMs could be easily obtained using different molds. In this work, various M-ZPMs with different shapes, such as cylinder, rectangular-prism, and donut shapes, were fabricated (see Figure 2d).

The microstructure of S-ZGMs and M-ZPMs was observed via SEM. Low-magnification SEM images, shown in Figures 3a, 3b, and 3c, respectively, reveal that all of the S-ZGM materials (S-ZGM-0.1, S-ZGM-0.2, and S-ZGM-0.3) are macroporous; they are composed of uniformly distributed zeolite gel and silica particles (10−400 nm) (see Figures 3a−c and the insets). The silica loading has a significant effect on the density of the S-ZGMs and the mechanical strength of the M-ZPMs. Much denser packing of the particles is observed in S-ZGM-0.3, whereas loosely packed particles are seen in S-ZGM-0.1 with lower silica loading. As a result, M-ZPM-0.3 exhibits much higher mechanical stability than M-ZPM-0.1.

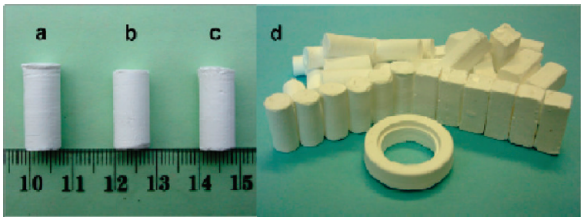

Figure 2. Photograph showing (a) a dried zeolite-gel monolith (ZGM-0.2), (b) a sintered monolith (S-ZGM-0.2), and (c) a macroporous NaP zeolite monolith (M-ZPM-0.2). Panel (d) shows a photograph of M-ZPMs with cylinder, rectangular-prism, and donut shapes.

As shown in the SEM images (Figures 3d, 3e, and 3f), macroporous M-ZPMs are composed of aggregated zeolitic particles, whose sizes are roughly in the range of 3−6 μm, 6−10 μm, and 7−13 μm for M-ZPM-0.1, M-ZPM-0.2, and M-ZPM-0.3, respectively. Close observations on the aggregated zeolitic particles reveal that M-ZPM-0.1 and M-ZPM-0.2 have hollow structures with a shell thickness of 0.6−1.3 μm and 1.0−2.0 μm (see Figures 3g and 3h), whereas M-ZPM-0.3 possesses a core/shell structure (see Figures 3i and 3l). The encapsulated core material in M-ZPM-0.3 consists of small particles, which are presumably unconsumed amorphous zeolite gel and silica. Extensive observations of the broken hollow zeolite particles of M-ZPMs revealed that their shells were intergrown with small NaP crystals (ca. 0.1−0.8 μm in size) and the adjacent shells were interconnected with each other (see Figures 3j, 3k, and 3l). Furthermore, as indicated by the arrows in Figures 3g−l, the hollow zeolite particles were interconnected, forming internal microwindows. Therefore, these intergrown adjacent shell structures are the backbone of robust zeolitic monoliths with high mechanical stability, and the internal open pore structure endows them with great guest encapsulation ability.

Because S-ZGM-0.1 and M-ZPM-0.1 had poor mechanical stability, the textural properties of mechanically stable S-ZGM-0.2 and S-ZGM-0.3, and M-ZPM-0.2 and M-ZPM-0.3, were characterized by mercury (Hg) porosimetry. As shown in Figure 4, both S-ZGM-0.2 and S-ZGM-0.3 exhibit a trimodal macropore size distribution with peaks centered at 0.2, 0.3, and 100 μm, respectively. However, after VPT crystallization, the macropores < 1 μm in size completely disappeared, whereas the larger macropore system (50−160 μm) was well-retained in the zeolitic monoliths. An additional macropore

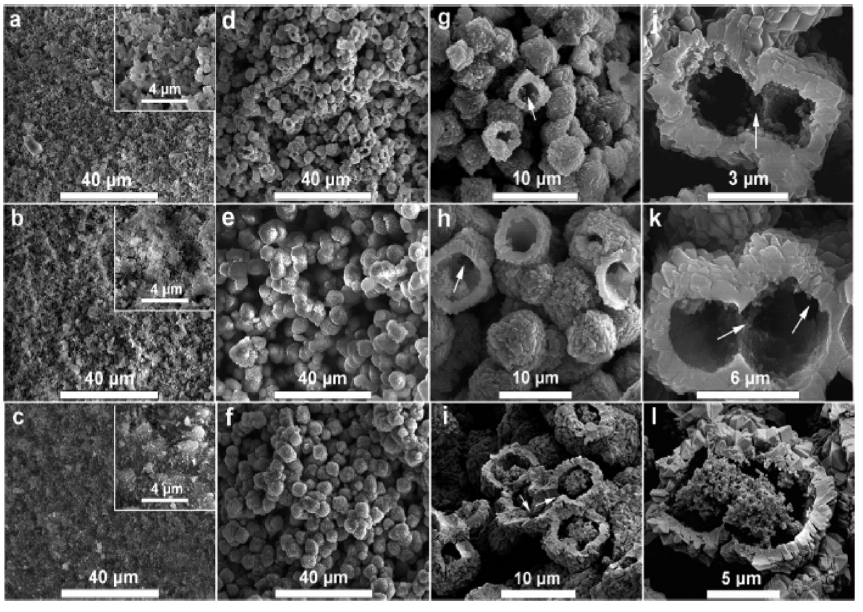

Figure 3. SEM images of (a) S-ZGM-0.1, (b) S-ZGM-0.2, and (c) S-ZGM-0.3. SEM images of M-ZPM-0.1 (panels (d), (g), and (j)), M-ZPM-0.2 (panels (e), (h), and (k)), and M-ZPM-0.3 (panels (f), (i), and (l)) also are shown. Panels (a)−(f) are low-magnification images; panels (g)−(l) and the insets in panels (a)−(c) are high-magnification images. The arrows added in panels (g), (h), (j), (k), and (l) indicate microwindows that connect the adjacent hollow NaP zeolite particles.

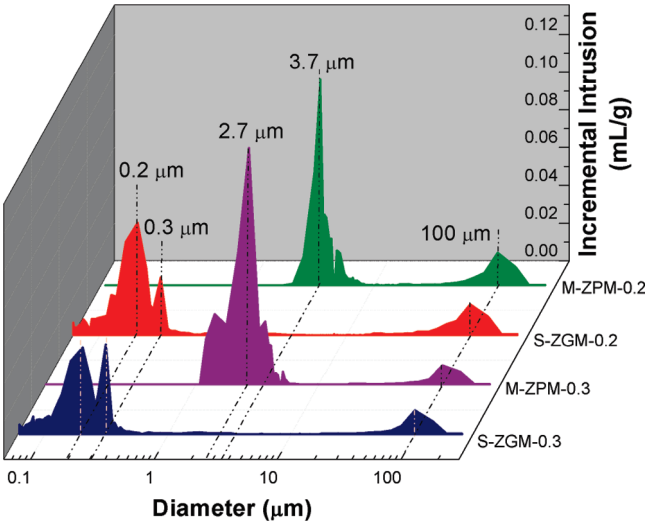

Figure 4. Pore size distributions of S-ZGM-0.2 and S-ZGM-0.3, and M-ZPM-0.2 and M-ZPM-0.3, as determined by mercury (Hg) porosimetry.

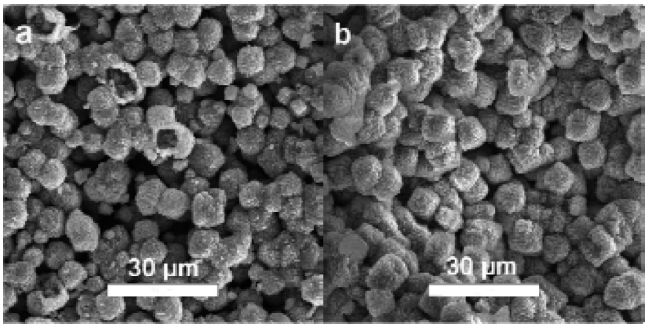

Figure 5. SEM images of (a) M-ZPM-0.2 and (b) M-ZPM-0.3 after 5 h of sonication. Both SEM images are shown in cross-sectional view.

system, with an average size of 3.7 μm for M-ZPM-0.2 and 2.7 μm for M-ZPM-0.3, was created after crystallization. As mentioned in the SEM studies, M-ZPM-0.2 constructed by intergrown hollow zeolite NaP particles possessed microcavities ca. 2−8 μm in size, which matches well with the pore size distribution of additional macropore system determined by Hg porosimetry. In addition, as revealed by SEM studies, the M-ZPM-0.3 consists of core/shell zeolite particles rather than hollow structures, which explains why it has a smaller average macropore size (2.7 μm) than M-ZPM-0.2 does.

To further evaluate the mechanical stability of M-ZPMs, the monolithic samples were subjected to vigorous sonication (60 kHz, 120 W). M-ZPM-0.2 and M-ZPM-0.3 remained intact after 5 h of sonication (Figure 5); however, M-ZPM-0.1 completely collapsed within 2 h. Both M-ZPM-0.2 and M-ZPM-0.3 were further soaked in water for 3 days, followed by secondary sonication for 3 h. Both monolithic shapes were retained, except a thin layer of powders was observed on the bottom of the bottle after the evaporation of water in the case of M-ZPM-0.2. This suggests that zeolitic monoliths prepared at a high silica loading exhibit reasonably good mechanical stability, because colloidal silica, which serves to bind zeolite gel particles together, assists the intergrowth of adjacent zeolitic shells during zeolite crystallization.

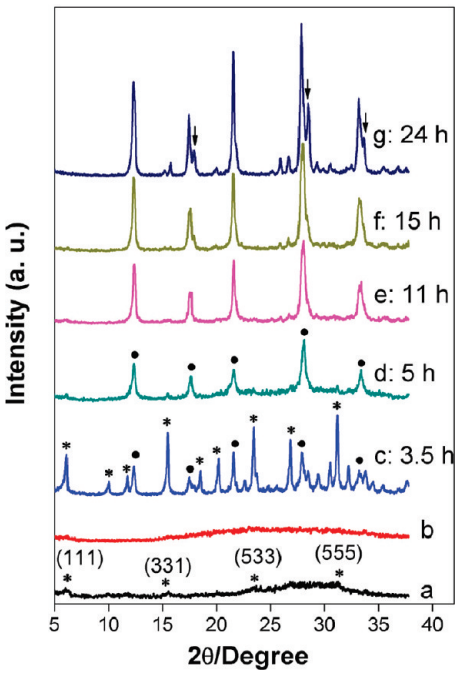

Figure 6. XRD patterns of dried zeolite gel (spectrum a), (b) S-ZGM-0 (spectrum b), and M-ZPM-0 after VPT synthesis for 3.5 h (spectrum c), 5 h (spectrum d), 11 h (spectrum e), 15 h (spectrum f), and 24 h (spectrum g). (Asterisk (∗) denotes FAU zeolite and solid circle (●) denotes NaP zeolite.)

Synthesis of Core/Shell and Hollow Zeolites without Adding Colloidal Silica. To study the effects of colloidal silica on the growth process of zeolite NaP, no colloidal silica was added in the aged zeolite gels (this sample is denoted M-ZPM-0). Individual zeolite NaP particles with core/shell and hollow structures were synthesized. Note that, without colloidal silica, the dried zeolite gel monoliths had very low mechanical strength and fell to pieces after the sintering process. To study the formation mechanisms of core/shell and zeolite NaP particles, the S-ZGM-0 pieces, which were composed of particles ∼3−5 mm in size, were used for subsequent crystallization. The samples were collected after VPT synthesis for 3.5, 5, 11, 15, and 24 h to examine their microstructures.

The XRD patterns of the S-ZGM-0 and VPT-treated samples are shown in Figure 6. The XRD pattern shows that S-ZGM-0 loses its semicrystalline FAU phase during sintering. After 3.5 h of VPT synthesis, the XRD results reveal that FAU (NaY) and GIS (NaP) phases coexist in the sample (see Figure 6c). However, NaY diffraction peaks (labeled with asterisks, ∗) are more intense than those NaP peaks, and the crystallization of NaY obviously dominates at this stage. From a thermodynamics perspective, zeolite crystallization is a progressive structural transformation process from a metastable phase to a more-stable phase.[32] In our case, the metaphase NaY zeolite first crystallizes and gradually transforms to the more-stable zeolite NaP phase after 5 h of VPT treatment, as indicated by XRD. As the crystallization time increases, e.g., from 5 h to 15 h, the intensities of NaP peaks further increase, suggesting the increase of the crystallinity of zeolite NaP. Note that the XRD diffraction peaks of samples subjected to VPT treatment for

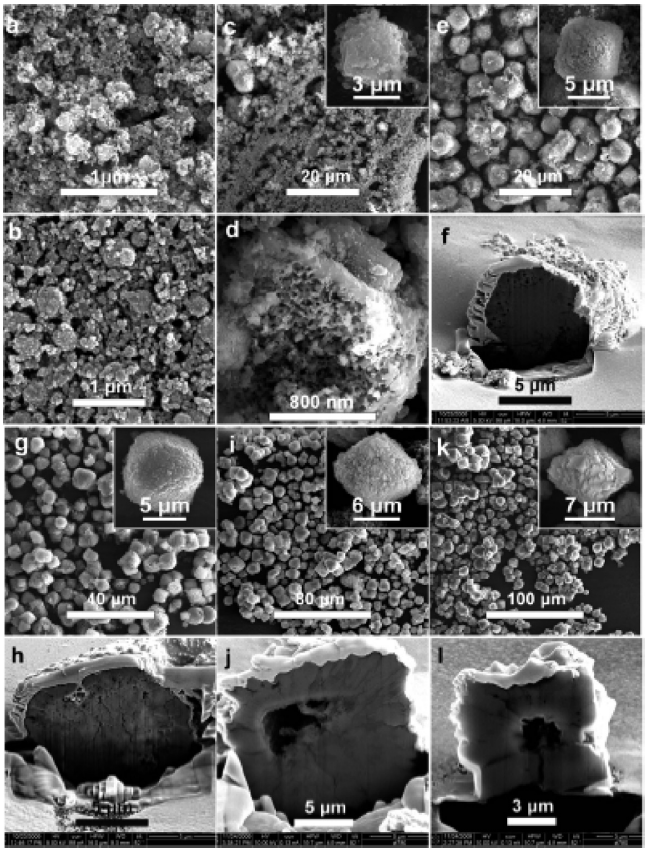

Figure 7. SEM/FIB-SEM images of (a) dried as-synthesized zeolite gel and (b) sintered zeolite gel (S-ZGM-0). Also shown are samples after VPT treatment for (c, d) 3.5 h, (e, f) 5 h, (g, h) 11 h, (i, j) 15 h, and (k, l) 24 h. The SEM image in panel (d) was taken on individual broken particles in thoroughly crushed 3.5-h samples. Panels (f), (h), (j), and (l) are the representative FIB-SEM images of the samples synthesized after VPT treatment for 5, 11, 15, and 24 h, respectively. The white coating on the top of the particles in FIB-SEM images is the platinum layer, which was deposited to protect the spherical particles from ion-beam damage during ion milling. The inset SEM images show the particles with typical morphologies at different stages.

24 h (or longer) are remarkably broadened, because of the incorporation of some proliferous peaks at 2θ angles of ~17.9°, 28.5°, and 33.7°, indicating the onset of structure rearrangement from existing cubic NaP to tetragonal topology (see Figure 6g).[24]

SEM and focused-ion-beam SEM (FIB-SEM) images of the samples taken at different growth stages are presented in Figure 7. Figure 7a shows that the as-synthesized zeolite gel consists of an abundance of nanoparticles 20−50 nm in size and a small portion of large aggregates ~300 nm in size. The calcination at 500 °C for 8 h leads to loosely packed particles without changing particle sizes. Uniform nanoparticles ~40 nm in size and some large particles ~400 nm in size are also observed in the high-resolution SEM image (see Figure 7b).

After VPT treatment for 3.5 h, some pseudo-spherical particles with diameters of 3−6 μm were produced (see Figure 7c). To further investigate the structure of the pseudo-spherical particles, 0.5 g of the sample was continuously crushed using an agate mortar and pestle for more than 15 min. Broken particles were examined by SEM, revealing that the particles have a core/shell structure,

Table 1. Elemental Compositions of the As-Synthesized Zeolite Gel and Samples after VPT Synthesis

synthesis time (h)	shell (Si/Al/Na/O)	core (Si/Al/Na/O)
0 (as-synthesized zeolite gel)	1.67/1/1.15/7.05	
3.5	1.66/1/1.12/7.02	
5	1.64/1/1.08/6.92	1.69/1/1.09/7.04
11	1.65/1/1.14/7.78	1.68/1/1.08/7.07
15	1.64/1/1.13/7.66	1.67/1/1.10/7.04
24	1.58/1/1.33/7.51	

which is composed of a porous core and a shell ~200 nm thick (see Figure 7d). After 5 h of VPT treatment, most particles grew to >5 μm in size (see Figure 7e), and the extensive observations on the individual particles indicate that there is a large number of closely packed small crystals with sharp edges and ~50−250 nm in size on the external surface of particles (see inset in Figure 7e). The representative FIB-SEM image of a typical particle shows that the regions between the shell and the core are highly porous (see Figure 7f). The interior materials are presumably undigested amorphous materials.

When the synthesis time was prolonged to 11 h, particles with an average size of ~8 μm were produced, their shells were composed of NaP crystallites with 300−500 nm in size (see Figure 7g and inset). The growth of the crystals on the shell from the interior for an extended synthesis time leads to an increase in shell thickness. The FIB-SEM image reveals a shell thickness of 0.5−1 μm and the porous structure of the core (see Figure 7h). When the reaction time was increased to 15 h, the shell grew to a thickness of 1−2 μm and the core, which served as a nutrient, was partly consumed, leading to typical core/shell structures at this stage (see Figure 7j). According to the XRD results, pure zeolite NaP was the only crystalline phase produced (see Figure 6f). Note that the NaP zeolite particles with increased sizes (5−12 μm) have a typical pseudo-rhombohedral shape, rather than the pseudo-spherical shape, probably because of the adjustment of surface crystal orientations during the Ostwald ripening process (see Figure 7i and inset). When the synthesis time was further increased to 24 h, hollow zeolite NaP particles with well-intergrown shell structures were formed, as shown in the FIB-SEM image (see Figure 7l). The hollow zeolite NaP particles finally had size of 6−15 μm (Figure 7k) and a shell thickness of 1.5−3.0 μm (Figure 7l). As indicated by the XRD result, the 24-h sample contained a small amount of tetragonal NaP zeolite phase, which was transformed from the existing cubic NaP zeolite phase (arrowed features in Figures 6a and 6g). Further prolongation of the heating time led to the progressive structural transformation to tetragonal zeolite NaP with a flowerlike morphology and a size over 15 μm (see Figure 1S in the Supporting Information). Elemental analysis was performed on both the shell and the core of the samples obtained at different stages of the VPT synthesis, and the results are listed in Table 1. The encapsulated core materials exhibit a slightly higher Si/Al ratio than their corresponding shells for the samples that were subjected to 5−11 h of VPT treatment; however, they were quite similar to that of dried zeolite gels. This was because of the incorporation of Al

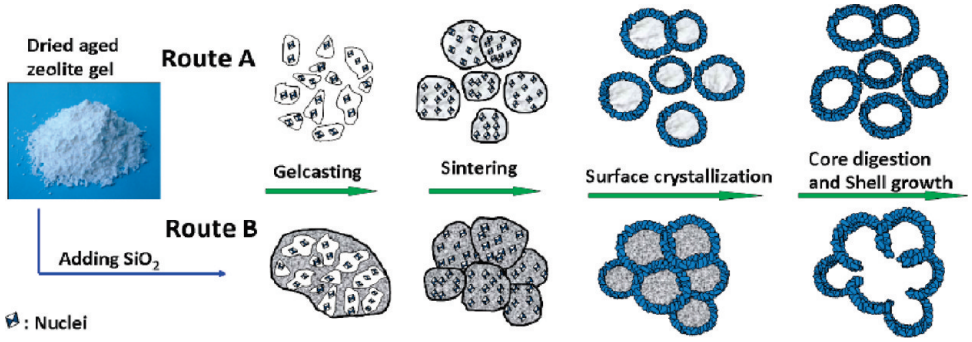

Figure 8. Schematic representation of the formation processes of the hollow NaP zeolite particles (M-ZPM-0, denoted as Route A) and macroporous NaP zeolitic monoliths (M-ZPM-0.1, M-ZPM-0.2, and M-ZPM-0.3, denoted as Route B).

into zeolite frameworks during crystallization of the shell. Considering that the zeolite NaP sample (M-ZPM-0) synthesized without amorphous silica is in the powder form, the 11-h and 24-h VTP samples were analyzed via a nitrogen sorption technique. The nitrogen sorption experiments show that both samples exhibit a very low BET surface area (< 5 m^2/g). This is because the samples are highly crystallized, and small-pore zeolite NaP does not absorb nitrogen molecules at liquid nitrogen temperature.

Formation Processes of Hollow NaP Particles and NaP Zeolitic Monoliths. Based on results presented above, the formation processes of hollow NaP particles and macroporous NaP zeolitic monoliths with or without colloidal silica are schematically illustrated in Figure 8. As described earlier, synthesis of sufficiently aged zeolite gel, high-temperature sintering, and VPT synthesis are key steps to successful formation of the hollow zeolite particles and robust zeolitic monoliths.

Specifically, the preparation processes start with the synthesis of aged zeolite gel, which is semicrystalline in nature, as indicated by XRD. The semicrystalline zeolite gel embedded with abundant FAU zeolite nuclei/domains allows for crystallization of NaP zeolite under VPT conditions within a very short period (e.g., 5 h). The zeolite transformation process takes slightly longer in the fabrication of macroporous zeolite NaP monolith (M-ZPMs), because of the addition of colloidal silica. In our experiments, however, without sufficient aging of the precursor, neither NaY nor NaP zeolite can be obtained under our synthetic conditions. Therefore, the employment of aged zeolite gel as the starting material is a prerequisite for the successful formation of NaP zeolites.

After the sintering process, the sample prepared without colloidal silica is in the form of loosely packed zeolite gel particles (Route A). The resulting monolith is very fragile and easily broken into small pieces during handling. However, in the presence of silica, the zeolite gel particles can be readily sintered together with silica, forming much denser monoliths with good mechanical strength (Route B).

During VPT synthesis, the zeolite crystallization presumably follows the recently reported surface-to-core crystallization mechanism.[18,33−35] At the early stage, a large number of individual pseudo-spherical particles are formed quickly by self-assembly of zeolite gel particles. Crystallization first occurs on the surfaces of these particles to form an initial shell structure, because of preferential and sufficient contact with water vapor in the VPT environment. It has been reported that zeolite nucleation preferentially occurs at the interfaces between the synthesis gels and solutions.[36−38] Such interfaces serve as ideal sites for zeolite nucleation and, thus, promote the primary crystallite aggregation in the surface-to-core growth direction. The surface particles then crystallize and aggregate by consuming the interiors as the VPT proceeds, leading to the crystallization of the shell inward to the core. Hollow zeolite structures are eventually developed by consuming zeolite synthesis gels in the center of aggregates via the solution-mediated process. By contrast, in Route B, because of closer packing of the aged gel particles and silica, adjacent zeolitic shells grow with each other, forming mechanically stable monoliths that are comprised of hollow zeolite aggregates with an internal open macropore system.

Encapsulation of Fe_3O_4 in M-ZPMs. Our synthesis strategy, combining gelcasting and VPT, offers an effective way to add functionalities to M-ZPMs. The synthesis of M-ZPM-0.2 with functional Fe_3O_4 (designated as M-ZPM-0.2-Fe_3O_4) is exemplified here. Fe_3O_4 nanoparticles (< 50 nm) were dispersed in the gelcasting suspension by ball milling until a uniform dark brown zeolite gel−SiO_2−Fe_3O_4 suspension was obtained. Fe_3O_4 functionalized macroporous zeolite NaP monoliths was thus prepared following the same synthetic procedure as those without Fe_3O_4.

As shown in Figure 9a, M-ZPM-0.2-Fe_3O_4 exhibits similar macroporous structures to that of M-ZPM-0.2. Close observations on the broken M-ZPM-0.2-Fe_3O_4 particles reveal that Fe_3O_4 particles exist inside hollow zeolite particles (see Figure 9b). This is further verified by

(33) Yao, J. F.; Li, D.; Zhang, X. Y.; Kong, C. H.; Yue, W. B.; Zhou, W. Z.; Wang, H. T. *Angew. Chem., Int. Ed.* **2008**, *47*, 8397–8399.
(34) Chen, X.; Qiao, M.; Xie, S.; Fan, K.; Zhou, W.; He, H. *J. Am. Chem. Soc.* **2007**, *129*, 13305–13312.
(35) Greer, H.; Wheatley, P. S.; Ashbrook, S. E.; Morris, R. E.; Zhou, W. Z. *J. Am. Chem. Soc.* **2009**, *131*, 17986–17992.
(36) Drews, T. O.; Katsoulakis, M. A.; Tsapatsis, M. *J. Phys. Chem. B* **2005**, *109*, 23879–23887.
(37) Nikolakis, V.; Vlacho, D. G.; Tsapatsis, M. *Microporous Mesoporous Mater.* **1998**, *21*, 337–346.
(38) Valtchev, V. P.; Bozhilov, K. N. *J. Am. Chem. Soc.* **2005**, *127*, 16171–16177.

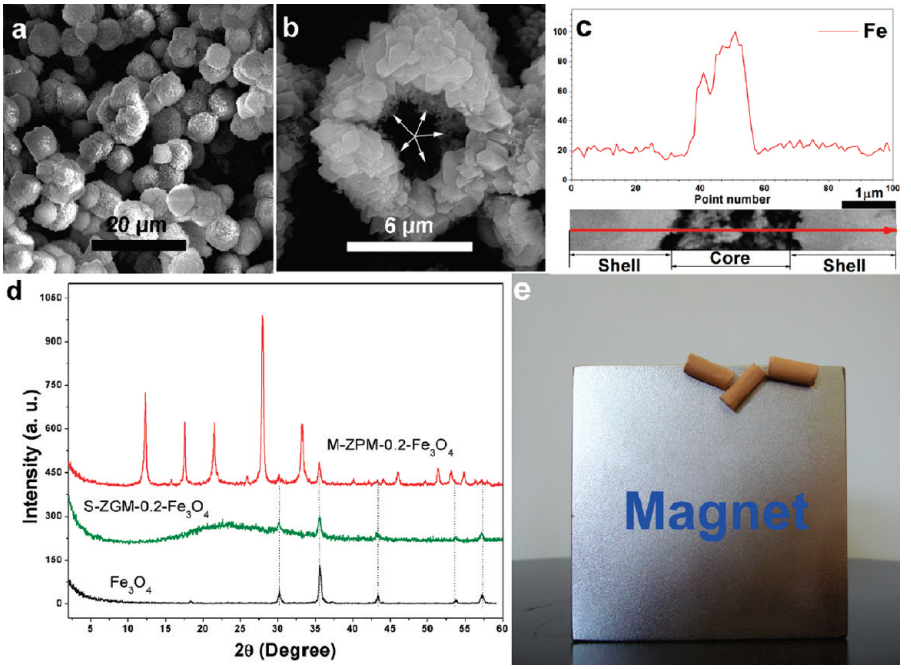

Figure 9. SEM images of (a) M-ZPM-0.2-Fe_3O_4 (cross-sectional view) and (b) a broken hollow NaP zeolite particle encapsulated with Fe_3O_4 (M-ZPM-0.2-Fe_3O_4); the white arrows indicate encapsulated Fe_3O_4 nanoparticles that are attached to the inner surface of the hollow zeolite NaP particles. Panel (c) shows an EDXS (line scan) graph of a crushed zeolite particle (shown at the bottom). Panel (d) shows XRD patterns of Fe_3O_4, S-ZGM-0.2-Fe_3O_4, and M-ZPM-0.2-Fe_3O_4. Panel (e) is a photograph of three M-ZPM-0.2-Fe_3O_4 cylinders attracted by a magnet.

performing EDXS analysis (line scan) on many individual broken zeolite particles along a shell−core−shell direction. A typical line-scan EDXS result is shown in Figure 9c. The zeolitic shells intergrown by zeolite NaP crystals do not produce FeK reflections, whereas strong peaks appear on the core, suggesting that Fe_3O_4 particles are mainly present in the core. In the XRD patterns (Figure 9d), characteristic Fe_3O_4 diffraction peaks are located at 2θ values of ~30.12°, 35.60°, 43.26°, 53.62°, and 57.22°, which further confirms the existence of Fe_3O_4 in both S-ZGM-0.2-Fe_3O_4 and M-ZPM-0.2-Fe_3O_4. Both XRD and SEM results indicate that the encapsulation of Fe_3O_4 in the monoliths does not have much influence on the crystallization of NaP zeolite with hollow structures. A very strong attraction between light brown M-ZPM-0.2-Fe_3O_4 cylinders and a magnet was observed (see Figure 9e); this proves that the Fe_3O_4 functionalized zeolitic monolith indeed has good magnetic properties. It should be possible to encapsulate other guest species into hollow zeolite structures using the synthesis strategy developed in the present work. In particular, the guest species that are not highly alkaline-stable could also be incorporated into hierarchical porous zeolitic structures, because the direct addition of guest species into a zeolite synthesis gel with high pH value is not required.

Conclusions

Hollow zeolite NaP particles and macroporous NaP monoliths were fabricated by combining the gelcasting process and vapor-phase-transport (VPT) synthesis. The mechanical stability, textural property, and chemical composition (Si/Al ratio) of the resulting zeolitic monoliths were adjusted by varying the silica loading. In the absence of silica nanoparticles, dispersible and individual core/shell and hollow zeolite particles were synthesized. Our study showed that the formation processes of hollow NaP zeolite structures follow surface (surface-to-core) crystallization and phase transformation mechanisms. Moreover, the macroporous NaP zeolitic monolith with controllable shapes and hollow zeolite structures are readily functionalized by incorporation of functional species, such as magnetic Fe_3O_4 particles, for potential applications as easy-to-recover adsorbents.

Acknowledgment. Financial support from the CSIRO Water for a Healthy Country Flagship and Australian Research Council is greatly acknowledged. Y.H. thanks the CSIRO for the postgraduate scholarship.

Supporting Information Available: Additional figures (PDF). This material is available free of charge via the Internet at http://pubs.acs.org.